Fearnbach Holly (Orcid ID: 0000-0002-4599-3339)

[4797]-□
Received: 17 April 2019 | Accepted 8 August 2019

NOTE

Evaluating the power of photogrammetry for monitoring killer whale body condition

Holly Fearnbach[1] | John W. Durban[2] | Lance G. Barrett-Lennard[3,4] | David K. Ellifrit[5] | Kenneth C. Balcomb III[5]

[1]SR3, SeaLife Response, Rehabilitation and Research, Seattle, Washington

[2]Marine Mammal and Turtle Division, Southwest Fisheries Science Center, National Marine Fisheries Service, NOAA, La Jolla, California

[3]Coastal Ocean Research Institute, Vancouver, British Columbia, Canada

[4]Zoology Department, University of British Columbia, Vancouver, British Columbia, Canada

[5]Center for Whale Research, Friday Harbor, Washington

Correspondence

Holly Fearnbach, SR3, SeaLife Response, Rehabilitation and

Research, 2255 Harbor Avenue SW Suite 101, Seattle, WA.

Email: hfearnbach@sealifer3.org

Aerial photogrammetry is increasingly being used to evaluate the body condition of free-ranging cetaceans (Christiansen et al., 2016, 2018; Durban et al., 2016; Fearnbach et al., 2018; Miller et al., 2012; Perryman & Lynn, 2002). This tool offers a noninvasive approach to quantitatively track the condition of recognizable individuals through time, potentially allowing for mitigation of anthropogenic impacts before they result in mortalities. An example of such longitudinal monitoring comes from our studies of endangered Southern Resident killer whales (*Orcinus orca*, SRKWs), for which we documented declining body condition of some individuals over a 5-year period between 2008 and 2013, including those that experienced subsequent mortality (Fearnbach et al., 2018). These data supported the hypothesis of limited prey availability as a key risk to recovery, as identified in conservation plans for SRKWs in both the United States and Canada (Fisheries and Oceans Canada, 2008; National Marine Fisheries Service, 2008).

Management actions to recover SRKWs are now focusing on maintaining and restoring priority runs of their primary prey, Chinook salmon (*Oncorhynchus tshawytscha*), and this requires

information on seasonal differences in body condition of SRKWs to relate to the timing of specific runs (NOAA and WDFW 2018). To assess body comparative condition before and after feeding on summer salmon runs, we launched an unmanned hexacopter from a boat platform (Durban et al., 2015) to collect digital aerial images of individually recognizable SRKWs (e.g., Fearnbach et al., 2011, 2018) during four alternating September and May sampling periods in 2015–2017. During each field effort the same camera (Olympus E-PM2) and flat lens (25 mm F1.8 Olympus M.Zuiko) were used to collect images from altitudes of 25–40 m to provide a water-level pixel resolution of 1–2 cm (Durban et al., 2015). This high resolution provided the potential to detect relatively subtle changes in morphometrics, but to assess changes in body condition we needed to develop and evaluate sensitive metrics that provided low measurement variability relative to the scale of change (i.e., high monitoring power).

When cetaceans become nutritionally stressed, they mobilize blubber fat reserves along the body, especially in larger whales (Miller et al., 2012), but they also lose adipose tissue behind the cranium (Bradford et al., 2012; Pettis et al., 2004). For

smaller cetaceans with limited blubber layers, reductions in this postcranial nuchal sack is an obvious measure of poor condition (Joblon et al., 2014) and can result in a “peanut head” appearance (Fearnbach et al., 2018). By examining aerial images of emaciated SRKWs prior to their deaths, our previous body condition metric (“HW ratio”; Figure 1) measured head width in pixels at a distance of 15% between the center of the blowhole and anterior insertion of the dorsal fin (BHDF) to document significant changes in body condition of individual SRKWs over a 5-year period (Fearnbach et al., 2018).

To control for growth in body size, we standardized this measure as a ratio of the BHDF length, but this potentially introduced measurement variability when defining the start of the dorsal fin and requires the entire back of the whale to be perpendicular to the image frame. In addition, it can be hard to accurately delineate the margins of the head against water disturbance when the whale surfaces. Furthermore, body proportions may change for growing whales, which may constrain power to detect meaningful changes in body condition over time. To further increase monitoring power, we again examined images

of emaciated whales to develop an eye patch (EP) ratio (Figure 1), which describes the fatness behind the cranium by measuring the distance in pixels between the inside edges of the white eye patches at a point 75% along the length of the eye patch length compared to between their anterior edges. We hypothesized that this measurement would be less sensitive to changes in the surfacing orientation of the whale, as unbiased measures only require the head to be perpendicular to the image plane, and also alleviates the requirement to identify the dorsal fin insertion. Similarly, by not having to standardize for body length, this measurement will be less be subject to changes in body proportions for growing whales. Furthermore, the measurements are taken between the inner margins of the eye patches, which are typically not obscured by water disturbance during surfacing (Figure 1).

To compare the relative monitoring power of these two photogrammetric metrics, we examined aerial images of the “J16” SRKW matriline, comprising six whales that were each photographed multiple times in each of the four consecutive seasonal sampling periods: September 2015, May 2016, September

2016, and May 2017 (Table 1). The J16 matriline included whales of widely varying ages and both sexes (Table 1), which ranged in size from 2–3 m for first year calves to ~7 m for an adult male (Fearnbach et al., 2011). Only high-quality images where the whales were in straight orientation (i.e., no tilt in the body axis) were selected: the white eye patches of killer provide very useful visual landmarks for assessing the whale orientation. Similarly, we attempted to select only images where the edges of the whale could be determined, and were not obscured by glare or wave action. Typically, more measurable-quality images were available for the EP ratio measure, indicating the practical merits of this metric. Furthermore, the variability in repeat EP ratio measurements was on average almost five times lower (average coefficient of variation, CV = standard deviation/mean = 0.005, range = 0.001–0.008) than the HW ratio (average CV = 0.021, range = 0.009–0.033). As a result, exploratory graphical analyses displayed an apparently greater power of the EP measurements to resolve seasonal trends (Figure 2).

To quantitatively demonstrate this increase in power, we

used a Bayesian hierarchical model to estimate the probability of a seasonal effect from these data, and to compare this probability across the two metrics. This model assumed a constant effect underlying condition changes between May and September, but did allow departures in individual condition from this seasonal trend in specific years, if supported by the data. The model was fit separately to both the EP and HW ratio data, and the measured ratio (R_{ijt}) for each whale i at each measurement j in each sampling period t was modeled as normally distributed with unknown mean (μ_{it}) and standard deviation (σ^S_{it}) that were estimated for each individual in each in each period. These sampling standard deviations were each assigned a Uniform (lower bound = 0, upper bound = 1) prior distribution that was updated when fit to data. The mean was specified by a model that was parameterized by an average level for each season ($q_{i=k}$), where k = 1 for September and k = 2 for May. Because of differences in age and sex of the whales, we expected them to have different body conditions (Fearnbach et al., 2018), and therefore also included individual effects (ε_{it}) to allow for

departures from the seasonal means: $R_{ijt} \sim N(\mu_{it}, \sigma^S_{it})$ $\mu_{it} = \theta_{i=k} + \varepsilon e_{it}$.

A vague Normal (mean = 0, standard deviation = 1,000) fixed effect was specified for each of the two seasonal terms θ, a Normal N(0, σ^p) prior distribution was specified for the individual effects and a Uniform (lower bound = 0, upper bound = 1) prior distribution was specified for the standard deviation of process error σ^p to allow departures from the seasonal levels to emerge, if supported by the data.

We used the WinBUGS software (Lunn et al., 2000) to implement Markov chain Monte Carlo (MCMC) sampling to estimate the posterior distribution for unknown parameters in the model. We based inference on 40,000 MCMC iterations after discarding a "burn-in" of 10,000 iterations prior to convergence of three different chains (Brooks and Gelman, 1998). The proportion of iterations for which the seasonal parameter $\theta_1 > \theta_2$ was interpreted as the probability that the average condition measurement of the whales was greater in September than May. This was the case when the model was fit to both the EP and the

HW ratio data, but for the HW ratio the distribution of θ_2 (May) significantly overlapped that of θ_1 (September), and the probability of a seasonal affect $p(\theta_2 < \theta_1)$ was only 0.70. In contrast the evidence of a seasonal effect was much stronger from the EP ratio data with $p(\theta_2 < \theta_1) = 0.96$ indicating less overlap in the posterior distributions (Figure 2).

Estimates of the individual departures from these means showed that the greatest changes in body condition were displayed by the three youngest whales, which notably had the poorest body condition in the May sampling periods (Figure 2). In contrast, the adult male had the largest EP ratio measurements and individual effect estimates in all four sampling periods. Adult male SRKWs are typically in the most robust condition of all the population (Fearnbach et al., 2018) despite the increased energy requirements associated with their larger size (Noren, 2011), likely in part the result of benefitting from prey sharing with their mothers and close kin to enhance inclusive fitness and increased foraging efforts (Foster et al., 2012a,b; Tennessen et al., 2019). The relatively poor condition of the youngsters, particularly in May, suggests

a time of low prey availability such that prey capture, sharing, and lactation from their mothers was not sufficient to maintain their body condition in the preceding winter months.

Our case study highlights an important component in aerial photogrammetry studies of cetacean morphometrics, namely the need to consider the power of measurements to fill the data gap in question. With the increasing use of unmanned aerial vehicles for collecting aerial imagery (Burnett et al., 2019; Christiansen et al., 2016, 2018; Durban et al., 2015, 2016), practitioners need to be mindful of both field and analytical approaches to ensure robust and useful photogrammetry. Key data collection requirements include selecting a flat lens to avoid image distortion, sensor and altitude considerations to achieve sufficiently high water-level resolution to resolve morphological differences, and precise altitude data if real scale is needed (see Christiansen et al., 2018; Dawson et al., 2017; Durban et al., 2015). Once these are met, large data samples can be collected at relatively low cost, placing a premium on data analysis and statistical inference. We not only investigated and compared the variability of two body condition

metrics at the level of empirical measurements, but also used a model to assess the consequence on our power to infer changes over time within a statistical framework. This has provided an informed basis for moving forward to provide longitudinal measurements of SRKW condition to support key recovery decisions.

Acknowledgments

This study was conducted with funding support from the NOAA, SR3, the SeaWorld and Busch Gardens Conservation Fund, the National Fish and Wildlife Foundation, Shell and SeaWorld. We are grateful to Lynne Barre for her support and encouragement and W. Perryman and D. LeRoi for their technical advice and field support. Jane and Tom Cogan, staff at the Center for Whale Research and Mark Malleson assisted in the field. Aerial and boat-based operations around whales were conducted under the authority of National Marine Fisheries Service Permits 16163 and 19091.

REFERENCES

Bradford A. L., Weller, D. W., Punt, A. E., Ivashchenko, Y. V., Burdin, A. M., VanBlaticom, G. R., & Brownell, R. L.

(2012). Leaner leviathans: Body condition variation in critically endangered whale population. *Journal of Mammalogy, 93*, 251–266.

Brooks, S. P., & Gelman, A. (1998). General methods for monitoring convergence of iterative simulations. *Journal of Computational and Graphical Statistics, 7*, 434–455.

Burnett, J. D., Lemos, L., Barlow, D. R., Wing, M. G., Chandler, T. E., & Torres, L. G. (2019). Estimating morphometric attributes of baleen whales with photogrammetry from small UASs: A case study with blue and gray whales. *Marine Mammal Science, 35*, 108–139.

Christiansen, F., Dujon, A. M., Sprogis, K. R., Arnould, J. P. Y., & Bejder, L. (2016). Noninvasive unmanned aerial vehicle provides estimates of the energetic cost of reproduction in humpback whales. *Ecosphere 7*(10), e01468.

Christiansen, F., Vivier, F., Charlton, C., Ward, R., Amerson, A., Burnell, S., & Bejder, L. (2018). Maternal body size and condition determine calf growth rates in southern right whales. *Marine Ecology Progress Series 592*, 267–281.

Dawson S. M., Bowman, M. H., Leunissen, E. & Sirguey, P. (2017).

Inexpensive aerial photogrammetry for studies of whales and large marine animals. *Frontiers of Marine Science 4*, 366.

Durban, J., Fearnbach, H., Barrett-Lennard, L. G., Perryman, W. L., & Leroi, D. J. (2015). Photogrammetry of killer whales using a small hexacopter launched at sea. *Journal of Unmanned Vehicle Systems, 3*, 131–135.

Durban, J. W., Moore, M. M., Chiang, G., Hickmott, L. S., Bocconcelli, A., Howes, G., … Leroi, D. J. (2016). Photogrammetry of blue whales with an unmanned hexacopter. *Marine Mammal Science, 32*, 1510–1515.

Fearnbach, H., Durban, J., Ellifrit, D., & Balcomb, K. C. (2011). Size and long-term growth trends of Endangered fish-eating killer whales. *Endangered Species Research, 13*, 173–180.

Fearnbach, H., Durban, J. W., Ellifrit, D. K., & Balcomb, K. C. (2018). Using aerial photogrammetry to detect changes in body condition in endangered Southern Resident killer whales. *Endangered Species Research, 35,* 175–180.

Fisheries and Oceans Canada. (2008). *Recovery strategy for the northern and southern resident killer whales* (Orcinus orca)

in Canada. Species at Risk Act Recovery Strategy Series, Ottawa, Canada. Retrieved from http://www.sararegistry.gc.ca/document/doc1341a/ind_e.cfm

Foster, E. A., Franks, D. W., Morrell, L. J., Balcomb, K. C., & Parsons, K. M. (2012a). Social network correlates of food availability in an endangered population of killer whales, *Orcinus orca*. *Animal Behavior, 83*, 731–736.

Foster, E. A., Franks, D. W., Mazzi, S., Draden, S. K., Balcomb, K. C., Ford, J. K. B., & Croft, D. P. (2012b). Adaptive prolonged postreproductive life span in killer whales. *Science 337*(6100), 1313.

Joblon, M. J., Pokra, M. A., Morse, B., & Harry, C. T. (2014). Body condition scoring system for delphinids based on short-beaked common dolphins (*Delphinus delphis*). *Journal of Marine Animals and Their Ecology, 7*, 5–13.

Lunn, D. J., Thomas, A., Best, N., & Spiegelhalter, D. (2000). WinBUGS - a Bayesian modelling framework: Concepts, structure and extensibility. *Statistical Computing*, *10*, 325–337.

Miller, C. A., Best, P. B., Perryman, W. L., Baumgartner, M. F.,

& Moore, M. J. (2012). Body shape changes associated with reproductive status, nutritive condition and growth in right whales *Eubalaena glacialis* and *E. australis*. *Marine Ecology Progress Series, 459*, 135–156.

National Marine Fisheries Service. (2008). *Recovery plan for Southern Resident killer whales* (Orcinus orca). Seattle, WA: National Marine Fisheries Service, Northwest Region. Retrieved from http://www.nmfs.noaa.gov/pr/pdfs/recovery/whale_ killer.pdf

NOAA and WDFS (Fisheries West Coast Region and Washington Department of Fish and Wildlife). (2018). *Southern Resident killer whale priority Chinook stocks report*. Retrieved from https://www.westcoast.fisheries.noaa.gov/publications/protected_species/marine_mammals/killer_whales/recovery/srkw_priority_chinook_stocks_conceptual_model_report___list_22june2018.pdf

Noren, D.P. (2011). Estimated field metabolic rates and prey requirements of resident killer whales. *Marine Mammal Science*, *27*, 60–77.

Perryman, W. L., & Lynn, M. S. (2002). Evaluation of nutritive

condition and reproductive status of migrating gray whales (*Eschrichtius robustus*) based on analysis of photogrammetric data. *Journal of Cetacean Research and Management, 4*, 155–164.

Pettis H. M., Rolland, R. M., Hamilton, P. K., Brault, S., Knowlton, A. R., & Kraus, S. D. (2004). Visual health assessment of North Atlantic right whales (*Eubalaena glacialis*) using photographs. *Canadian Journal of Zoology*, *82*, 8–19.

Tennessen, J. B., Holt, M. M., Hanson, M. B., Emmons, C. K., Giles, D. A., & Hogan, J. T. (2019). Kinematic signatures of prey capture from archival tags reveal sex differences in killer whale foraging activity. *Journal of Experimental Biology, 222*(3), jeb191784.

TABLE 1 Summary statistics for two metrics of body condition obtained from aerial images of the J16 matriline of Southern Resident killer whales over four sampling periods. The sex and birth year for each of the six whales is shown along with the number of images (*n*) that were measured for both metrics and the coefficient of variation (CV = standard deviation/mean) for repeat measurements of each whale within each sampling period. The eye patch (EP) ratio is the ratio of the separation between the inside of the eye patches at their anterior end relative to their separation at 75% of the eye patch length. The head width (HW) ratio is the ratio of head width at 15% of the length between the center of the blowhole and anterior insertion of the dorsal fin (BHDF) relative to BHDF.

Whale	**Sex, Born**	**September 2015**		**May 2016**		**September 2016**		**May 2017**	
		EP	**HW**	**EP**	**HW**	**EP**	**HW**	**EP**	**HW**
		n	***n***	***n***	***n***	***n***	***n***	***n***	***n***
		(CV)	**(CV)**	**(CV)**	**(CV)**	**(CV)**	**(CV)**	**(CV)**	**(CV)**
J16	F, 1972	17	11	10	8	10	10	11	11
		(0.005)	(0.020)	(0.008)	(0.025)	(0.006)	(0.011)	(0.005)	(0.017)
J26	M, 1991	12	11	9	9	12	6	12	14
		(0.005)	(0.021)	(0.005)	(0.019)	(0.004)	(0.020)	(0.005)	(0.022)

J36	F, 1999	10 (0.004)	3 (0.020)	12 (0.005)	11 (0.023)	12 (0.005)	10 (0.012)	13 (0.004)	14 (0.027)
J42	F, 2007	11 (0.004)	10 (0.028)	5 (0.005)	3 (0.022)	12 (0.004)	5 (0.024)	8 (0.004)	7 (0.020)
J50	F, 2014	4 (0.006)	3 (0.009)	5 (0.003)	6 (0.033)	14 (0.004)	5 (0.028)	5 (0.007)	6 (0.021)
J52	M, 2015	3 (0.008)	6 (0.010)	2 (0.006)	3 (0.032)	14 (0.003)	5 (0.020)	8 (0.003)	7 (0.013)

FIGURE 1 Aerial images of J36 (left) showing the measurements for the eye patch ratio (EPR, proportion of “EP Top” and “EP Bottom”) and J16 (right) showing the measurements for the head width (HW) ratio (ratio of HW and blowhole to dorsal fin (BHDF)). Both are indicators of nutritional condition, allowing changes in condition to be detected on both a seasonal and annual level.

FIGURE 2 Plots showing change in two metrics of body condition for six whales in the J16 matriline of Southern Resident killer whales. Left: eye patch (EP) ratio is the ratio of the separation between the inside of the eye patches at their anterior end relative to their separation at 75% of the eye patch length. Right: head width (HW) ratio is the ratio of head width at 15% of the length between the center of the blowhole and anterior insertion of the dorsal fin (BHDF) relative to BHDF. In the top plots solid lines join estimates of the same individual for each sampling period, legend displays color for each individual detailed in Table 1, circles show mean measurements and vertical lines represent the standard deviation of measurements during each sampling period. The bottom panels

are density plots of the posterior distribution for seasonal effect, averaged across individuals; one distribution is shown for each of the May and September parameters as the result of fitting a Bayesian hierarchical model to the EP and HW data separately.

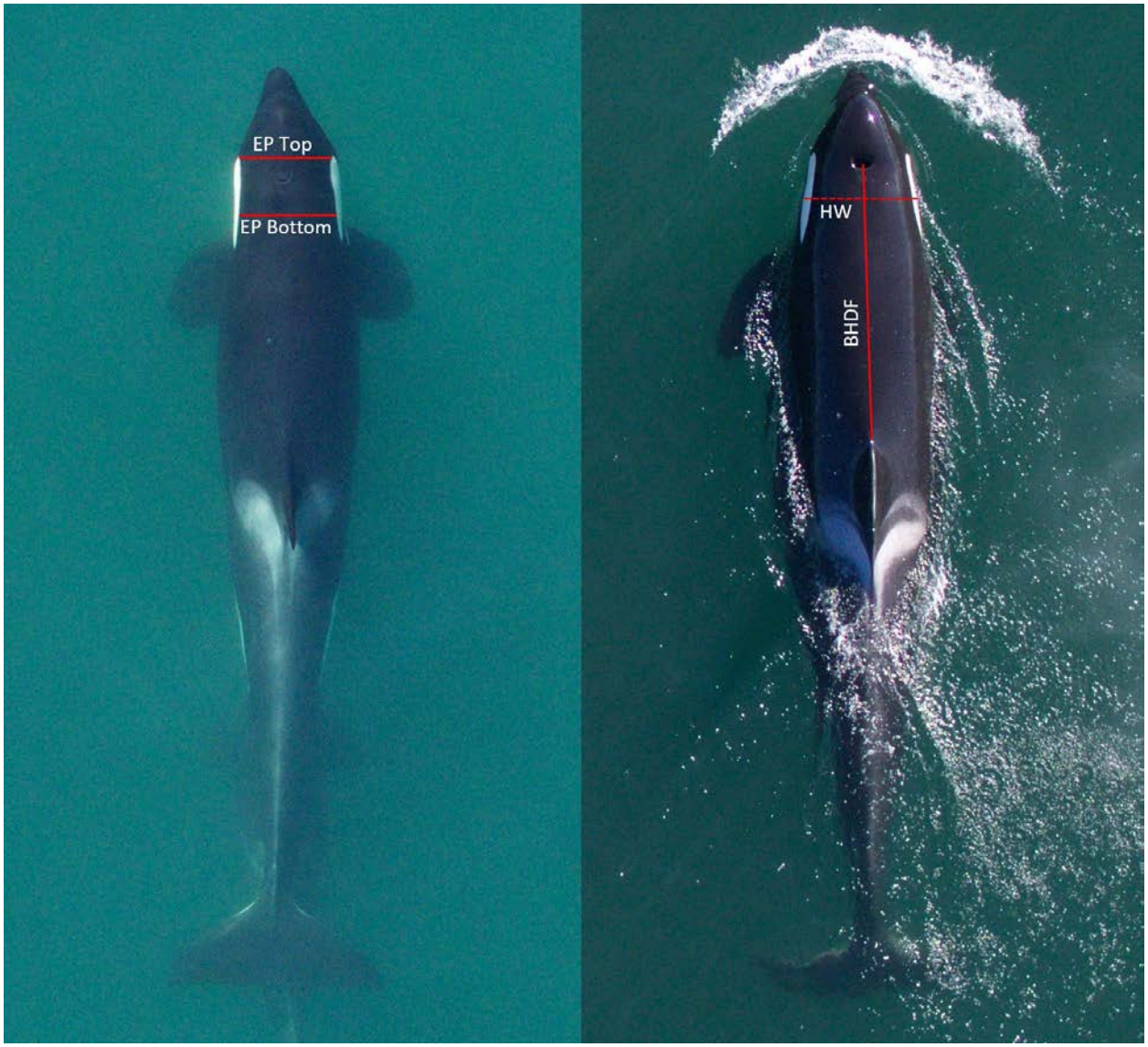

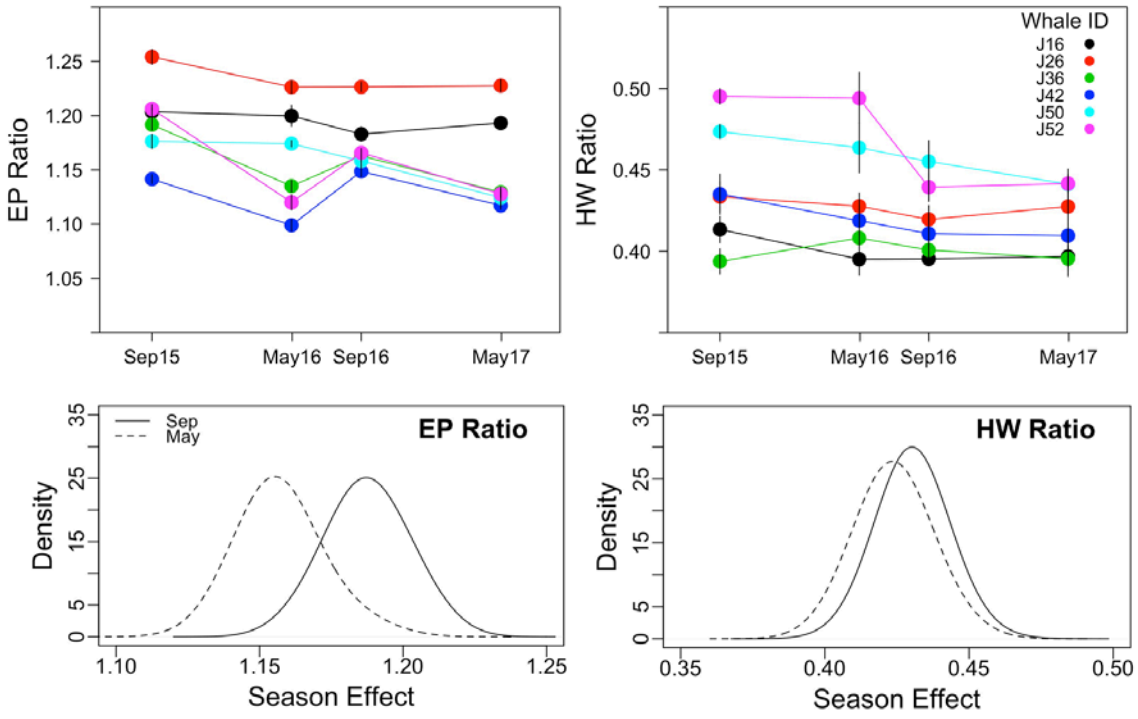

MMS_12642_4797_Figure 1.tif

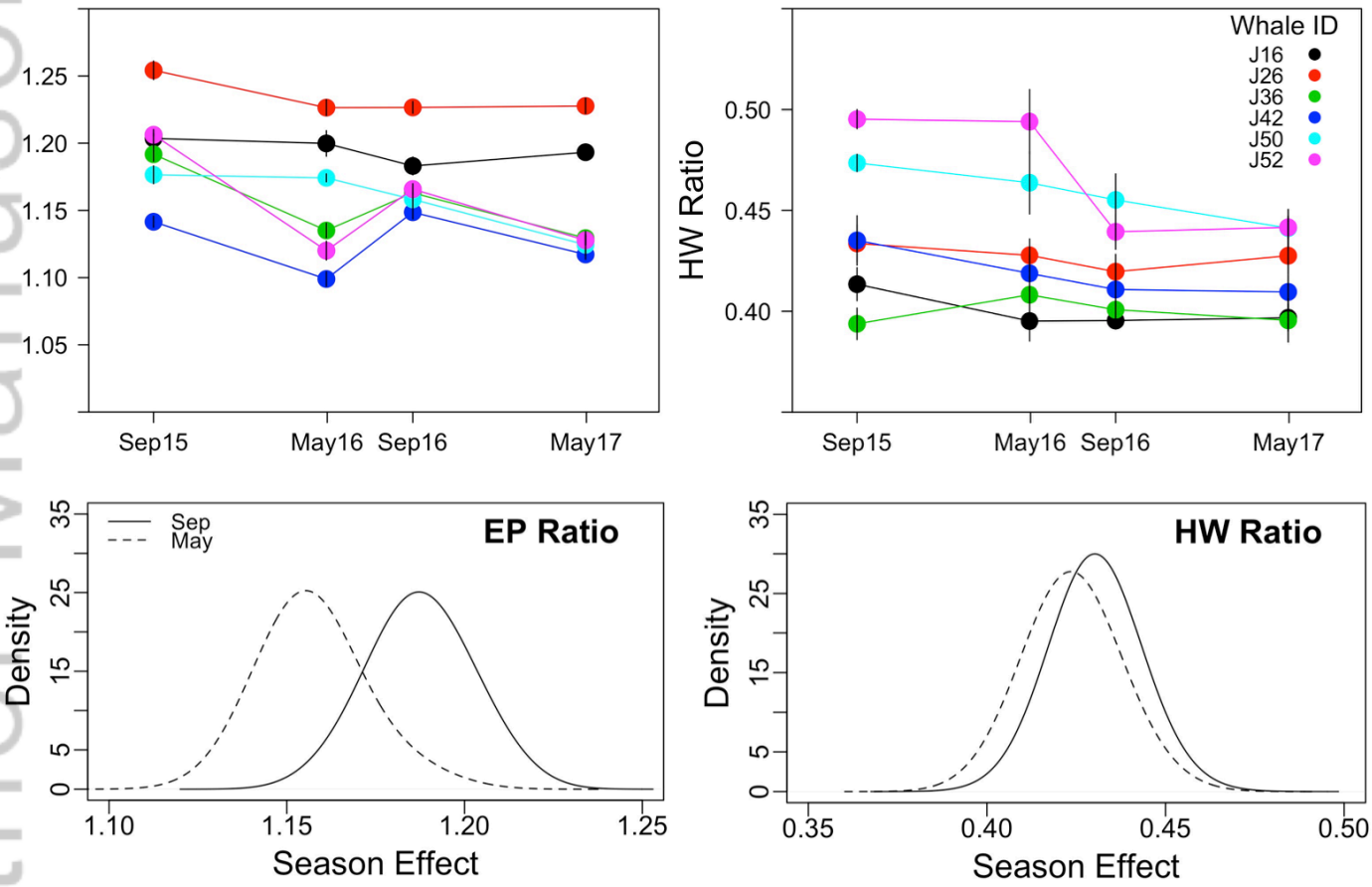

MMS_12642_4797_Figure 2.tiff